2018 IEEE/RSJ International Conference on Intelligent Robots and Systems (IROS)
Madrid, Spain, October 1-5, 2018

A comparison of assistive methods for suturing in MIRS

Giuseppe Andrea Fontanelli[1], Guang-Zhong Yang[2], Bruno Siciliano[1]

***Abstract*— In Minimally Invasive Robotic Surgery (MIRS) a robot is interposed between the surgeon and the surgical site to increase the precision, dexterity, and to reduce surgeon's effort and cognitive load with respect to the standard laparoscopic interventions. However, the modern robotic systems for MIRS are still based on the traditional telemanipulation paradigm, e.g. the robot behaviour is fully under surgeon's control, and no autonomy or assistance is implemented. In this work, supervised and shared controllers have been developed in a vision-free, human-in-the-loop, control framework to help surgeon during a surgical suturing procedure. Experiments conducted on the da Vinci Research Kit robot proves the effectiveness of the method indicating also the guidelines for improving results.**

I. INTRODUCTION

Medical robotics represents one of the fast growing sectors in the medical device industry. In [1] the future trends in assistive and autonomous robotic surgery are discussed, identifying six level of autonomy for medical robotics; from level 0 (*no autonomy*) to level 6 (*fully autonomy*) through different levels of assistance.

In this work, we aim at discussing a comparison between the firsts three levels of autonomy (*no autonomy*, *robot assistance*, *task autonomy*) cited in [1] focusing on the surgical suturing procedure.

Suturing is still one of the most critical and delicate tasks in Minimally Invasive Robotic Surgery (MIRS) because it is time demanding, high dexterity is required and the risks of causing damage to organs and/or tissues is elevated. This procedure can be technically demanding even for a skilled surgeon, mostly because of the reduced workspace, the high precision required, the lack of haptic perception and the complexity induced by artificial vision feedback [2]. An analysis of the needle-tissue interaction force and of the optimal needle trajectory to perform the stitch has been proposed in [3], [4]. As a result, using a circular shape needle commonly used in laparoscopic interventions, the optimal needle trajectory, reducing tissue damages for both needle insertion and extraction, is a path locally tangential to the needle shape. However, in telemanipulation, the execution of the required needle trajectory is not always possible mainly for the following reasons: (i) the needle is not always visible particularly during the needle extraction; (ii) directly controlling the 6-degrees-of-freedom (DOFs) of the slave manipulator in both position and orientation is a quite a complex task; (iii) the required movement on the master side to execute the task is often burdensome forcing the surgeon to perform uncomfortable wrist rotations; (iii) the lack of haptic feedback leads the surgeon to not understand the applied damages [5].

This problem can be overcome by using the enhanced precision of the robot to perform the required path in an automatic or semi-automatic paradigm. Automation in suturing has been an active research topic for many years. Different methods have been developed at different levels of assistance. Starting from the higher level of assistance in [6] and [7], an automatic multi-throw framework and a supervised paradigm have been developed. A different approach has been proposed in [8] based on learning by demonstration performing a non-rigid registration between the demonstration trajectory, generated by the human, and a test scenario. Although the fully autonomous or supervised approaches are promising, the technological limitation, e.g. wound and needle tracking, in an unstructured environment, such as in laparoscopic surgery, and the regulatory concerns make clinical translation of this technology challenging.

Hence, in this work, we choose to use a vision-free, surgeon-in-the-loop control paradigm in which the vision correction is directly provided by the surgeon's perception while the robotic assistance is completely designed in a relative frame. Taking inspiration from the work in [9], in which virtual fixtures are used to constrain both the position and the orientation of the users on performing the needle insertion and the knot tying, we make a step forward proposing two new shared control strategies and two intuitive master-slave mappings focusing on the stitching procedure. Moreover, to comparatively analyze the impact on the users of different levels of assistance, also a supervised controller has been proposed in the same vision-free surgeon-in-the-loop framework.

A. Contributions

The main contribution of this paper includes: (i) design of a simple and effective interactive stitch planner, (ii) design of three supervised/assisted control strategies for surgical suturing; (iii) a detailed user study to compare the controller performances using the da Vinci Research Kit (dVRK) robotic platform. The rest of this paper is organized as follows: In Section II we present preliminary methods used in our implementation; in Section III we present the assisted surgical suturing framework and the developed control strategies; Section IV present the experimental and test setup; Section V discusses the results obtained; while Section VI concludes the paper.

[1]The authors are with the Interdepartmental Center for Advances in Robotic Surgery (ICAROS) University of Naples Federico II. First author e-mail: giuseppeandrea.fontanelli@unina.it

[2]The author is with the Hamlyn Centre for Robotic Surgery, Imperial College London.

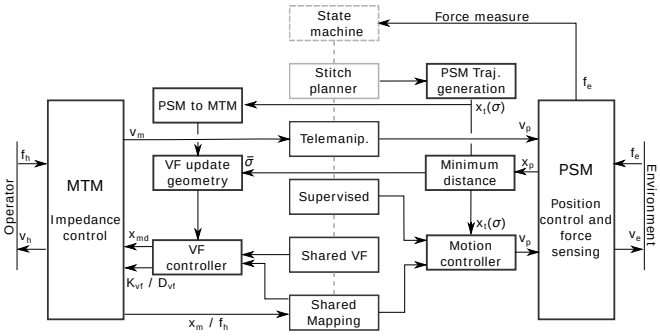

Fig. 1. Proposed master-slave control structure. MTM: Master Tool Manipulator, PSM: Patient Side Manipulator.

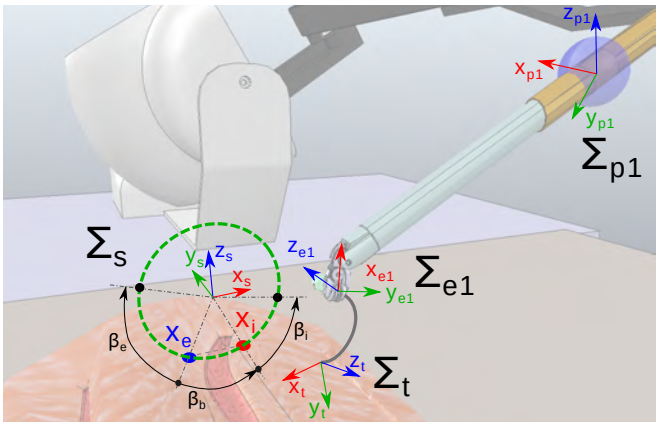

Fig. 2. Slave side frames disposition. With Σ_s, Σ_t, Σ_{e1}, Σ_{p1} we indicate respectively the stitch frame, needle-tip frame, end-effector frame of the PSM1 and base frame. With x_e and x_i we indicate the insertion and extraction poses. β_b, β_i, β_e represent respectively the base, insertion and extraction angles described in Sub. Section III-A.

II. PRELIMINARIES

In this section, we illustrate the methods used to implement the presented control strategies on a surgical master-slave system.

A. Master-slave configuration

A common practice in robotic teleoperation is to have an impedance controlled master robot and a position/velocity controlled slave robot. This allows a precise motion of the slave robot and a full control on the master to implement advanced control strategies for human-robot interaction.

1) Master Impedance Control: Considering a n-degree of-freedom (DoF) robot and defining a task space vector $\boldsymbol{x} \in \mathbb{R}^r$, with $r \leq n$, the goal of an impedance control is to impose the following impedance dynamics to the robot behavior [10]:

$$\boldsymbol{M}\ddot{\tilde{\boldsymbol{x}}} + \boldsymbol{D}\dot{\tilde{\boldsymbol{x}}} = \boldsymbol{f}_{\mathrm{h}} + \boldsymbol{f}_{\mathrm{c}}(\cdot), \tag{1}$$

where $\tilde{\boldsymbol{x}} = \boldsymbol{x}_{\mathrm{d}} - \boldsymbol{x}$, with $\boldsymbol{x}_{\mathrm{d}}$ being the "virtual" reference, specifying the desired value for the task space variables of the robot, $\boldsymbol{M} \in \mathbb{R}^{r\times r}$ and $\boldsymbol{D} \in \mathbb{R}^{r\times r}$ are positive definite inertia and damping matrices. Moreover, $\boldsymbol{f}_{\mathrm{h}} \in \mathbb{R}^r$ is the vector of the external wrenches applied by the human user while $\boldsymbol{f}_{\mathrm{c}}(\cdot) \in \mathbb{R}^r$ is the vector of controlled wrenches, e.g. generated to implement a virtual guidance as described in the next sections. In this work, the design of the desired impedance behavior has been supported by the results presented in [11], where the dVRK Master Tool Manipuators (MTMs) and Patient Side Manipulators (PSMs) dynamic model have been identified.

Moreover, on the dVRK master the external force is not directly measurable, hence force estimation must be performed [12]. In this work, we use the nonlinear dynamic observer proposed in [13]. This method allows the estimation of the unknown external forces without the need of measuring the usually noisy acceleration signal. In details, the estimated external forces $\hat{\boldsymbol{f}}_{\mathrm{h}}$ can be computed as: $\hat{\boldsymbol{f}}_{\mathrm{h}} = \boldsymbol{J}^{-T}(\boldsymbol{q})\boldsymbol{r}$, were, $\boldsymbol{r} \in \mathbb{R}^n$ is the residual vector defined in [13] and $\boldsymbol{J}(\boldsymbol{q}) \in \mathbb{R}^{r\times n}$ denotes the robot Jacobian[1]. We will hereafter consider $\boldsymbol{f}_{\mathrm{h}} = \hat{\boldsymbol{f}}_{\mathrm{h}}$ to simplify the notation.

[1]If the robot is redundant a suitable pseudoinverse of the Jacobian transpose must be considered.

2) Slave external force estimation: The proposed control framework and the following performance analysis make an extensive use of the slave force measure, as discussed in the following sections. In this work, we choose to measure the external slave force $\boldsymbol{f}_s \in \mathbb{R}^3$ making use of our recently presented force sensor integrated into the trocar of the dVRK robot [5]. This solution allows measuring the interaction forces between the surgical instrument and the environment without any changes to the instrument structure. Our sensor is able to measure the two components of the force lying on the plane orthogonal to the instrument axis with a resolution up to 0.1N as reported in [5]. The third component has been estimated using the non-linear observer described in the previous section supported by the PSMs dynamic model identified in [11].

III. ASSISTED SUTURING FRAMEWORK

In this section, the proposed framework is presented in details focusing on the adopted methodology for the stitch planning and presenting the three proposed assisted stitching control strategies (see Fig. 1 for a schematic visualization of the proposed controllers).

A. Interactive stitch planning

In the proposed approach all the trajectories are planned in the relative stitch frame Σ_s (see Fig. 2). To this purpose, an interactive stitch selection strategy has been implemented. Using the slave side force measure and the surgeon's visual perception in the loop we design an effective method that can be locally used to interactively select the stitch frame without other visual input. In details, the norm of the force measured with our trocar force sensor has been used to classify the gripper-tissue interaction. Particularly, a threshold ρ_s has been defined experimentally considering both the tissue elasticity parameter, in order to minimize the tissue deformation during the selection, and the sensor resolution. Basically, the entrance and the exit point for each stitch have been selected touching the tissue sequentially at

the desired insertion and extraction points $\boldsymbol{x}_i$ and $\boldsymbol{x}_e$, with the PSM gripper fingers orthogonal to the tissue surface. At each selection, the slave end-effector pose $\boldsymbol{x}_p \in \mathbb{R}^6$ has been recorded and, from that, the fingers normal unit vector $\boldsymbol{r}_{fi} \in \mathbb{R}^3$ and $\boldsymbol{r}_{fi} \in \mathbb{R}^3$ has been calculated respectively for the insertion and extraction points. Therefore, the Σ_s frame (see Fig. 2) has been obtained by choosing: (i) the $\boldsymbol{x}_s$ axis along the direction from $\boldsymbol{x}_e$ to $\boldsymbol{x}_i$; (ii) the $\boldsymbol{y}_s$ axis as cross product $\boldsymbol{y}_s = \boldsymbol{x}_s \times (\boldsymbol{r}_{fi} + \boldsymbol{r}_{fe})$, (ii) the axis $\boldsymbol{z}_s = \boldsymbol{x}_s \times \boldsymbol{y}_s$ to have an orthonormal frame; (iv) the frame origin in the center of the circle (with radius equal to the chosen needle radius) lying on the plane defined by $\boldsymbol{x}_s$ and $\boldsymbol{z}_s$ and passing through the points $\boldsymbol{x}_i$ and $\boldsymbol{x}_e$.

After defining the stitch frame, the stitch planner deals with calculating the needle tip trajectory, in Σ_s, to approach and execute the needle insertion/extraction. The goal is to minimize the tissue stress during the stitch execution. To this purpose, based on the result presented in [3], [4], we define a circular tip trajectory tangent to the circular shape of the needle. More in details, defining an insertion and an extraction angle β_i and β_e, considering the angle β_b as shown in Fig. 2 and a needle with radius r, the tangential path to perform the stitch insertion/extraction is calculated as parametric pose, with respect to the scalar curvilinear abscissa $\sigma \in [0, 1]$,

$$\boldsymbol{x}_t^s(\sigma) = [\boldsymbol{p}_t^s(\sigma),\ \boldsymbol{\Phi}_t^s(\sigma)]^T \in \mathbb{R}^6 \tag{2}$$

where, in this implementation:

$$\boldsymbol{p}_t^s(\sigma) = [r\cos(-\beta\sigma + \theta_i),\ 0,\ r\sin(-\beta\sigma + \theta_i)]^T$$

and $\boldsymbol{\Phi}_t^s(\sigma) = [0,\ -\pi/2 + \theta_i + \beta\sigma,\ 0]^T$ with $\beta = \beta_b + \beta_i + \beta_e$, $\theta_i = \beta_b/2 + \beta_i - \pi/2$ (see Fig. 2).

This trajectory is used to plan the PSM motion or to plan the virtual fixture assistance as discussed in the next sections.

B. Control strategies

In this work, we compare the standard fully telemanipulation paradigm with three different assistance strategies.

1) Fully telemanipulation: In this modality, the user is given the full control of the 6-DoFs of the slave robot. This can be achieved by implementing the classic velocity coupling between master and slave

$$\boldsymbol{v}_p = \begin{bmatrix} s\boldsymbol{R}_m^p & \boldsymbol{0} \\ \boldsymbol{0} & \boldsymbol{R}_m^p \end{bmatrix} \boldsymbol{v}_m \tag{3}$$

where, $\boldsymbol{v}_m = [\dot{\boldsymbol{p}}_m, \boldsymbol{\omega}_m]$ and $\boldsymbol{v}_p = [\dot{\boldsymbol{p}}_p, \boldsymbol{\omega}_p]$ [2] are respectively the master and the slave velocity, s is the scalar scale factor and $\boldsymbol{R}_m^p \in \mathbb{R}^{3\times3}$ is the rotation matrix between the MTM base frame "m" and the PSM base frame "p".

2) Supervised control: In our framework, the supervised control represents the higher level of autonomy given to the robot for the stitch execution. In this control paradigm, the slave robot motion is fully autonomous, when performing the stitch trajectory, while the user can supervise the robot by starting and stopping the controller as described in Sec. IV-A.

[2] $\dot{\boldsymbol{p}}$ and $\boldsymbol{\omega}$ represent respectively the linear and the angular velocity.

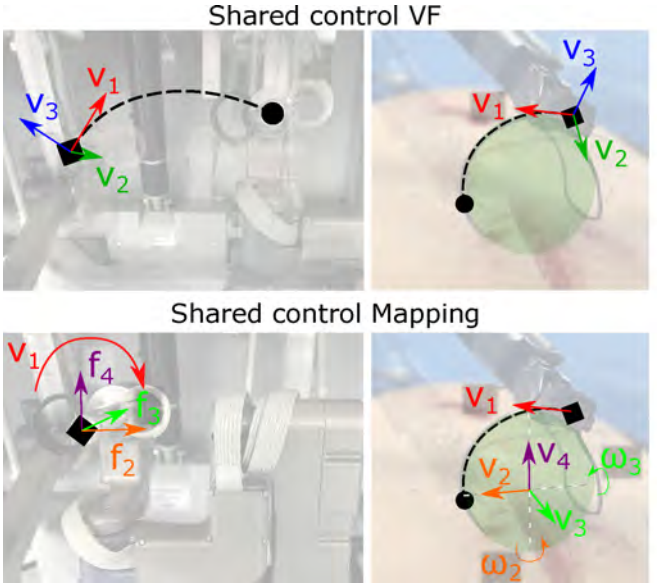

Fig. 3. A visualization of the mapping between the master DoFs and the slave DoFs in the two implemented shared controllers.

The described behaviour has been obtained by considering a trapezoidal velocity profile temporal law [10] for the parameter $\sigma(t)$ in (2) and projecting, at each time interval, the desired tip velocity $\boldsymbol{v}_t^s(\sigma(t))$ to the slave robot end effector:

$$\boldsymbol{v}_p(\sigma(t)) = \begin{bmatrix} \boldsymbol{R}_s^p & -\boldsymbol{R}_s^p \boldsymbol{S}\left(\boldsymbol{R}_p^s \boldsymbol{p}_p - \boldsymbol{p}_t^s\right) \\ \boldsymbol{0} & \boldsymbol{R}_s^p \end{bmatrix} \boldsymbol{v}_t^s(\sigma(t)) \tag{4}$$

where, $\boldsymbol{R}_s^p \in \mathbb{R}^{3\times3}$ is the constant rotation matrix between the stitch frame Σ_s and the PSMs base frames Σ_{p1} or Σ_{p2} (see Fig. 2); $\boldsymbol{p}_p$, $\boldsymbol{p}_t^s$ are the position vectors related to the PSMs direct kinematics and position vectors related to the needle tip in frame stitch respectively. Notice that, the two PSMs have been calibrated using the efficient hand-eye calibration approach proposed in [14] to find the relation between the two robots base frames. Finally, $\boldsymbol{S}(\cdot)$ represents the skew symmetric matrix operator.

3) Shared control using virtual fixtures (VF): In this control strategy, we propose a guidance virtual fixture (GVFs) [15] method to constrain the user in position along the specified path while leaving his/her orientation free. On the other hand, on the slave side, the position is controlled in telemanipulation by the master while the orientation is automatically imposed. In Fig. 3 the defined mapping is visualized: the motion along the VF on the master side (v_1) is mapped into a tangential motion of the needle tip along the needle circular shape. Moreover, the slave motion in the two directions orthogonal to the path (v_2, v_3) is even possible by applying a force $\boldsymbol{f}_h \neq \boldsymbol{0}$ on the master. The described behaviour has been obtained by considering a spatial variation law for the trajectory parameter σ based on the minimum distance $\tilde{x}_t$ between the actual needle tip pose $\boldsymbol{x}_{te}^s$ and the curve $\boldsymbol{x}_t^s(\sigma)$. In details, given the actual needle tip position, the curvilinear abscissa $\bar{\sigma}$, corresponding to the minimum distance, is calculated with respect to the trajectory

$\boldsymbol{x}_t^s(\sigma)$ as:

$$\bar{\sigma} = \arg\min_{\sigma} \quad \|\boldsymbol{W}_p(\boldsymbol{x}_t^s(\sigma) - \boldsymbol{x}_{te}^s)\| \tag{5}$$

where, $\boldsymbol{W}_p = \text{diag}(1,1,1,0,0,0)$ is a selection matrix used to consider only the position error. In the case of a circular path the minimum distance can be obtained in closed form. The mathematical derivation is not reported here for brevity. Finally, a low-pass filter has been used to smoothen the $\hat{\sigma}(t)$ behavior and avoid possible switching when the needle tip is near the circle center: $\bar{\sigma}_f(s) = \bar{\sigma}(s)/(1 + sk_fT)$ where T is the control sampling time and k_f is a positive scalar gain.

Therefore, to obtain the desired behaviour the virtual reference on the master side $\boldsymbol{x}_{md}$ is calculated by opportunely projecting, at each time interval, $\boldsymbol{x}_t^s(\bar{\sigma_f})$ on the master side by integrating the following velocity mapping between the slave and the master pose:

$$\boldsymbol{v}_{md}(\bar{\sigma_f}) = \begin{bmatrix} \frac{1}{s}\boldsymbol{R}_s^m & -\frac{1}{s}\boldsymbol{R}_s^m \boldsymbol{S}\left(\boldsymbol{R}_p^s \boldsymbol{p}_p - \boldsymbol{p}_t^s\right) \\ \boldsymbol{0} & \boldsymbol{R}_s^m \end{bmatrix} \boldsymbol{v}_t^s(\bar{\sigma_f}) \tag{6}$$

where, $\boldsymbol{R}_s^m = \boldsymbol{R}_p^m \boldsymbol{R}_s^p$.

Hence, the impedance controlled master manipulator described in (1), endowed with an attractive GVF constraint enforcement method given by a spring-damper force:

$$\boldsymbol{f}_{\text{c}}(\cdot) = \boldsymbol{f}_{\text{vf}}(\tilde{\boldsymbol{x}}_m, \dot{\tilde{\boldsymbol{x}}}_m) = -\boldsymbol{K}_{\text{vf}}\tilde{\boldsymbol{x}}_m - \boldsymbol{D}_{\text{vf}}\dot{\tilde{\boldsymbol{x}}}_m \tag{7}$$

is described by:

$$\boldsymbol{M}\ddot{\tilde{\boldsymbol{x}}}_m + \hat{\boldsymbol{D}}\dot{\tilde{\boldsymbol{x}}}_m + \boldsymbol{K}_{\text{vf}}\tilde{\boldsymbol{x}}_m = \boldsymbol{f}_{\text{h}}, \tag{8}$$

with $\hat{\boldsymbol{D}} = \boldsymbol{D} + \boldsymbol{D}_{\text{vf}}$ and

$$\boldsymbol{K}_{\text{vf}} = \text{diag}\,[k,k,k,0,0,0] \tag{9}$$

chosen diagonal to constrain the user motion only in position.

On the other hand, at the slave side the desired velocity $\boldsymbol{v}_p$ has been obtained considering the reference provided by the master, for the position, and by the programmed trajectory for the orientation:

$$\boldsymbol{v}_p(\bar{\sigma_f}) = \begin{bmatrix} s\boldsymbol{R}_m^p & \boldsymbol{0} \\ \boldsymbol{0} & \boldsymbol{R}_m^p \end{bmatrix} \begin{bmatrix} \dot{\boldsymbol{p}}_m \\ \boldsymbol{\omega}_{md}(\bar{\sigma_f}) \end{bmatrix} \tag{10}$$

4) Shared control using an orientation mapping: The aim of this control strategy is to constrain the motion of the needle tip along the defined trajectory commanding the desired coordinate on the path, defined by $\bar{\sigma}$, using the master orientation. The described behaviour has been obtained by considering the parameter σ as a differential projection of the angular velocity around the axis of the master gripper and by using Eq. (4) to obtain the slave velocity.

$$\dot{\sigma} = \boldsymbol{W}_m(\boldsymbol{R}_e^m)^T \boldsymbol{\omega}_m \tag{11}$$

where $\boldsymbol{R}_e^m$ is the rotation matrix related to the master direct kinematics used to evaluate the angular velocity in frame end effector and $\boldsymbol{W}_m = [0,0,1]$ is a selection matrix used to consider only the orientation around the master gripper axis. In this case, the master manipulator is controlled in impedance to have its position fixed in the space and the orientation free. To this purpose, the VF stiffness is imposed as described in Eq. 9. This choice is motivated by the fact that in this way the orientation of the user is completely free and only the last joint needs to be rotated. This allows an intuitive control of the needle by minimizing the effort needed to reach the correct orientation.

Moreover, in order to enable the user to correct possible errors in the stitch pose, due to imprecision in the stitch selection or due to the tissue motion, we design a stitch pose adaptation strategy. Basically, the pose transformation between the adapted stitch frame $\Sigma_{\hat{s}}$ and the current stitch frame Σ_s can be obtained by integrating the force at the master side to have a 3-dimensional motion. We choose to use only the force information without considering the torque information due to the noisy and less predictable master torque estimation. Hence, the camera pedal has been used to switch between the position and the orientation adaptation. In details, we consider the velocity $\boldsymbol{v}_{\hat{s}}^s$ of the adapted stitch frame w.r.t Σ_s as:

$$\boldsymbol{v}_{\hat{s}}^s = \begin{bmatrix} -\gamma \boldsymbol{W}_p \boldsymbol{f}_h \\ (\gamma - 1)\boldsymbol{W}_o \boldsymbol{f}_h \end{bmatrix} \tag{12}$$

where, $\boldsymbol{W}_p = [\Delta\boldsymbol{p}, \boldsymbol{0}] \in \mathbb{R}^{3\times 6}$ is a selection matrix used to extract only the position terms and $\boldsymbol{W}_o \in \mathbb{R}^{3\times 6}$ is:

$$\boldsymbol{W}_o = \begin{bmatrix} \Delta\Phi_1 & 0 & 0 & & \\ 0 & 0 & \Delta\Phi_3 & \boldsymbol{0}_{3x3} & \\ 0 & 0 & 0 & & \end{bmatrix} \tag{13}$$

and γ a binary coefficient used to activate the position and the orientation adaptation; $\Delta\boldsymbol{p} = [\Delta p_1, \Delta p_2, \Delta p_3]$ and $\Delta\boldsymbol{\Phi} = [\Delta\Phi_1, 0, \Delta\Phi_3]$ are respectively the position and orientation steps obtained experimentally. Finally, an element-wise force threshold of $\rho_m = 2$N has been used to avoid undesired motion during the stitch execution.

IV. EXPERIMENTS

This section aims at proving with both performances metrics and user study whether and which type of assistance is useful to perform the stitch task minimizing the tissue damages and at the same time the surgeon's workload.

A. Experimental set-up

The experimental setup is composed by the full dVRK [16] robotic platform provided with a console composed by two master side manipulators (MTMs) and a stereo-visor; two patient side manipulators (PSMs) and an endoscopic arm (ECM) provided with a stereo camera. The provided ROS-based functions included in the *"dvrk-ros"* API have been used to read the robots state and to control (at 5ms) the slave and the master robots respectively in position and in torque. The stiffness value k in (9) has been opportunely filtered with a first order filter $\dot{\tilde{k}} + K_p\tilde{k} = 0$ with $\tilde{k} = k_d - k$ and $K_p > 0$ to smoothly adapt the stiffness variation, where, we chose $k_d = 300$N/m for needle insertion and $k_d = 150$N/m

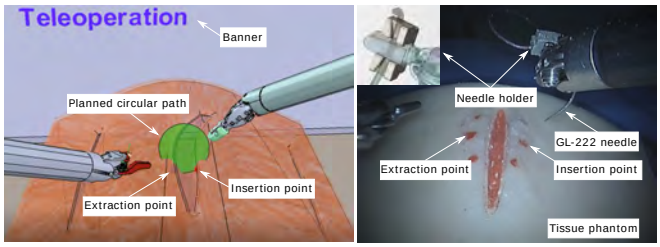

Fig. 4. Description of the experimental setup. Left: Augmented Reality (AR) feedback. Right: setup used in the proposed experiments.

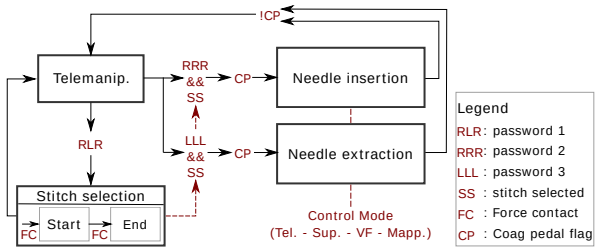

Fig. 5. Description of the password-based state machine.

for needle extraction.[3] A surgical suturing phantom has been used to simulate a human wound on which two red dots have been marked as a guide for the stitch selection. A large needle driver instrument from Intuitive Surgical Inc. has been used to move a GL-222 needle with an external diameter of 17.5 mm. In order to have the full control of the needle position a metal printed needle holder (see Fig. 4) has been used whose design was inspired by [6]. Finally, a VREP simulator of the slave set-up has been used for the preliminary tests and for augmented reality (see Fig. 4).

Moreover, as described in Fig. 5, we choose to use "gripper passwords" to give the user control of the high-level state machine. More in details, three different passwords have been used to switch between: (i) *telemanipulation*; (ii) *stitch selection*; (iii) *needle insertion*; (iv) *needle extraction*. Each password can be commanded when the robot is not in telemanipulation, e.g. CP $= 0$ (CP: coag pedal flag), by simply pressing a combination of the master right gripper (R) or master left gripper (L). Each control, including the standard *telemanipolation*, is activated by the pressure of the coag pedal (CP $= 1$) and is stopped when it is released returning at the state *telemanipolation*.

B. Test setup

The user study has been performed by volunteer users recruited from a population of both engineers and surgeons in the Hamlyn Center of Imperial College of London. A total of ten right-handed subjects (average age 26) completed the experiment. All participants had at least one previous experience with the da Vinci platform. Each participant spent about 20 minutes, performing different suture in telemanipulation, for training both the robotic platform and the stitch framework, before to start the experiment. None of the participants has neurological or vision disorder that may negatively affect the results. The conducted experiment is composed of the following phases: (i) the surgeon selects the stitch using the provided force-enabled method; (ii) the surgeon executes the stitch performing both insertion and extraction of the needle by using, in a random sequence, the four described control paradigms. In each experiment the user is fully autonomous, receiving all the information regarding the stitch frame, the actual control active and instruction about the action to undertake directly in augmented reality by messages and visual information in the VREP simulated environment.

[3]Is a worth noticing that since the stiffness matrix is not constant the passivity of the system is not proved [12] and hence instability problems can occur. Following the results presented in [17] by injecting a constant damping into the system $\boldsymbol{D}_{\text{vf}} > \alpha \boldsymbol{M}$, where $\boldsymbol{M}$ is the master robot inertia matrix and α is such that $\boldsymbol{K}_{\text{vf}}(t) - 2\alpha \boldsymbol{K}_{\text{vf}}(t)$ is negative semi-definite, the passivity is guaranteed. Hence, by choosing opportunely the K_p filter parameter we can bound the stiffness variation $\dot{\boldsymbol{K}}_{\text{vf}}(t)$ and avoid to inject undesirable high damping.

V. RESULTS

In Fig. 6 the timeline of the experiment is shown. In details, we report the needle tip position and orientation in stitch frame in Figs. 6(a,b)[4], the master robots (MTMR, MTML) position and orientation in Figs. 6(c,d,e,f), the PSM1 out-of-tangent needle tip force in Fig. 6(g) and the time evolution of the stiffness in Fig. 6(h). The behaviour of the four control paradigms, described in the previous sections, is clearly visible showing the different mapping between the master and the slave. In details it is possible to notice that: (i) the master needs to be moved in both position and orientation when the telemanipulation controller is active, (ii) it is fixed when the supervised controller is used, (iii) it needs to be moved only in position, leaving the orientation free, using the supervised VF control paradigm while only the orientation needs to be controlled considering the shared mapping control paradigm. This translates into different levels of workload as will be discussed in the next section.

A. Controllers performance evaluation

As evaluation metric, for each stitch (insertion and extraction), we calculate the execution time and the applied forces on the tissue. More in details, we measure the out-of-tangent forces acting on the needle tip during the needle insertion as $\boldsymbol{f}_{nt} = \|\boldsymbol{W}_f \boldsymbol{R}_p^t \boldsymbol{f}_s\|$, where, $\boldsymbol{f}_s$ is the slave force obtained as described in Sec. II-A.2, $\boldsymbol{R}_p^t \in \mathbb{R}^{3\times3}$ is a projection matrix and $\boldsymbol{W}_f \in \mathbb{R}^{2\times3}$ is an opportune matrix used to select only the y_t and z_t components. In Figs. 7, 8 are shown the results of one of the experiments performed in the user study by a trainee surgeon. In details, the out-of-tangent force for the needle insertion is reported in Fig. 7 and the executed needle tip trajectory respectively during the needle insertion and the needle extraction sub-task are shown in Fig. 8. It is clearly possible to notice that the executed trajectory in both tasks performed in telemanipulation is not following the correct circular path. Indeed, during the insertion usually the surgeons firstly moves following a linear

[4]To have a clearer visualization, the trajectories are plotted only when the needle is gripped and the insertion or extraction trajectory is performed.

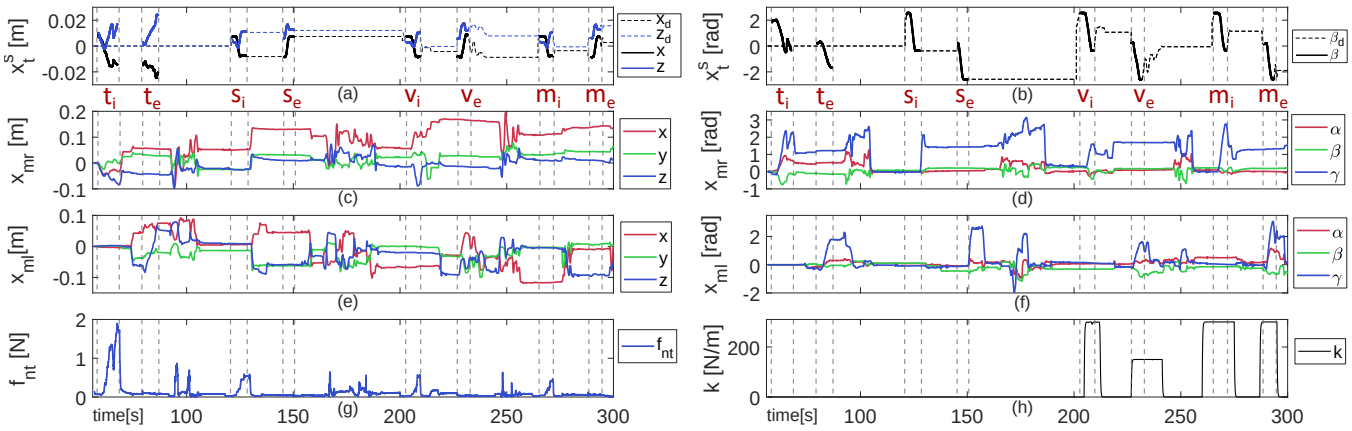

Fig. 6. Experiment timeline. (t, s, v, m): telemanipulation, supervised, virtual fixtures, mapping controllers; (i, e): insertion, extraction phase. (a,b) needle tip position and orientation displacement, (c,d) MTMR position and orientation, (e,f) MTML position and orientation, (g) PSM1 out-of-tangent needle tip force, (h) master stiffness. We indicate with α, β and γ the orientation expressed in Euler angles.

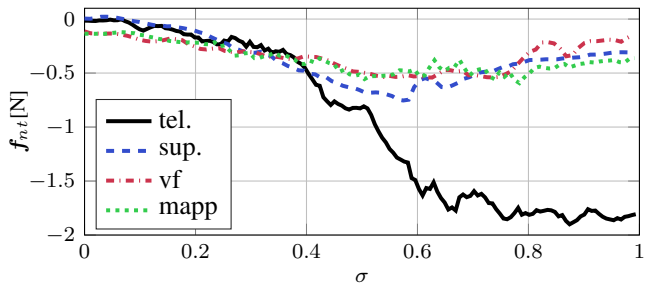

Fig. 7. Out of tangent needle tissue interaction force in the four control cases. σ represents the curvilinear abscissa.

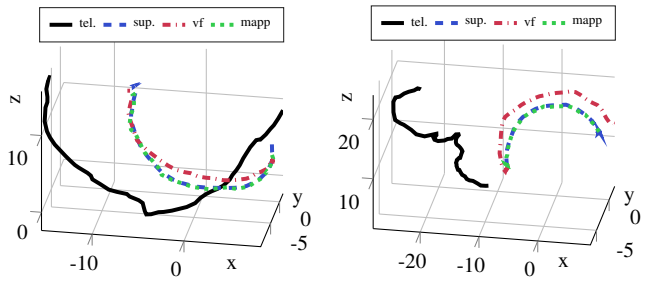

Fig. 8. Needle tip trajectory during the needle insertion (top) and the needle extraction (bottom). The insertion is from the right to the left, the extraction is from the left to the right.

path and after the needle is rotated (as was also reported in [9]). Furthermore, during needle extraction, the behaviour is still worst showing that in the 60% of the cases a linear trajectory in the opposite direction of the needle shape is performed. Moreover, the average measured time and the out-of-the-tangent needle force is double when the task is performed in telemanipulation compared to the use of one of the proposed assisted controllers(see Fig.9).

Comparing the three proposed control strategies, we can see an improved precision using the supervised and the shared mapping controllers while the time consumption and the out of tangent forces show similar results. This is because, with respect to the supervised and the shared mapping strategies, in the shared VF controller only the position is constrained and hence bigger errors in the needle trajectory are possible while, on the other hand, the automatic orientation control allows having bounded forces in all the cases. Finally, although the supervised controller shows the better results in precision and exerted forces, we measured a success rate less than 75% considering our implementation. The failure cases are due to an incorrect needle position inside the gripper, a bad stitch selection or because the needle has not gone out on the other tissue side preventing a correct supervised needle extraction. On the other hand, the two shared strategies show a better success rate enabled by the possibility to correct, on-line, the performed trajectory.

B. *Subjective user evaluation*

We have asked the users to complete a NASA TLX workload survey [18] to evaluate the level of workload required. In the analysis four parameters have been chosen by the user (Effort, Frustration, Mental, Physical) while the Temporal and Performance parameter has been calculated as discussed in the previous section. The result of the experiment in shown in Fig. 10. We can notice that for the three proposed control strategies the resulted workload is significantly lower with respect to the standard telemanipulation paradigm. Better results are shown considering the supervised controller, with less workload for the surgeon and also better performances. However, as discussed before, this control is less robust and more prone to failure. Moreover, the two shared control solutions show similar results with a slightly better performances and less effort for the *Mapping* controller respect to the solution based on virtual guidance. At the question: "This type of assistance can be useful for both the needle insertion and extraction?" the answer has been positive in 70% of the cases for the needle insertion and 90% for the needle extraction. Moreover, we have asked whether with the proposed strategies the user felt to have less control of the robot and the answer has been: 55%, 21% and 23% positive respectively for the supervised, shared VF and shared mapping controls but never in a negative sense. Also for the supervised strategy, the possibility of the user to

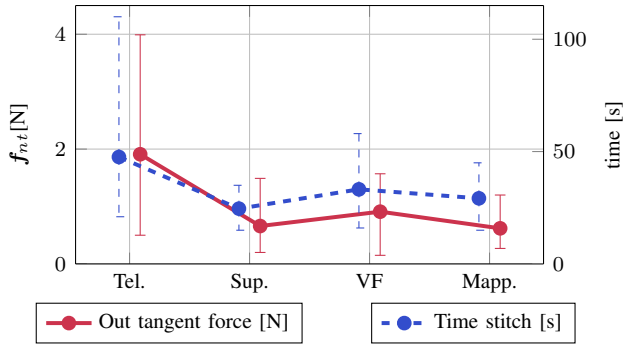

Fig. 9. Performance evaluation of the four proposed controllers considering time spent for each stitch and out-of-tangent force exerted on the tissue.

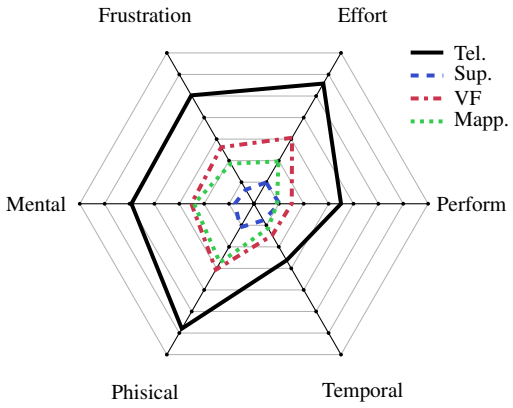

Fig. 10. Nasa TLX workload survey using the four control strategies. Values near the center indicate better results.

switch easily between autonomous and telemanipulation state give the sensation to not loose completely the system control. Finally, at the question: "Which is the preferred controller?" the result have been 20%, 20% and 60% respectively for the supervised, shared VF and shared mapping. Hence, instead of the slightly improved precision and the reduced workload provided by the supervised controller, the users feel to have better performance, control, and less workload when at least one degree of freedom, for the needle motion, is under his/her control. Moreover, the possibility to correct the stitch frame pose on-line has been appreciated giving the sensation of a better control of the task.

VI. CONCLUSION AND FUTURE WORKS

In this work, a comparison between four control paradigm for the surgical suturing procedure has been presented. A novel force-enabled stitch selection and a password based state machine permit an interactive, easy and fast control of the task. Moreover, three novel surgeon-in-the-loop control strategies have been presented with different levels of assistance. Two new kinematic mappings have been proposed to share the DoFs required to complete the stitching task with the robot reducing the required effort, mental load and time consumed. The results of our user study show significant better performance with the proposed assisted controllers with respect to the standard telemanipulation paradigm reporting also a reduced workload when at least one degree of freedom is left to the surgeon. In future works, we plan to evaluate other shared control strategies exploiting the presence of additional DoFs introduced by our recent results regarding a new laparoscopic tool for continuous needle reorientation [2]. Moreover, computer vision techniques will be employed for needle and wound tracking in order to improve augmented reality techniques and the robustness against on-line changes in the environment.

REFERENCES

[1] G. Z. Yang, J. Cambias, K. Cleary, E. Daimler, J. Drake, P. E. Dupont, N. Hata, P. Kazanzides, S. Martel, R. V. Patel, V. J. Santos, and R. H. Taylor, "Medical robotics - regulatory, ethical and legal considerations for increasing levels of autonomy," *Science Robotics*, vol. 2, no. 4, pp. 309–314, Mar. 2017.

[2] G. A. Fontanelli, M. Selvaggio, L. R. Buonocore, F. Ficuciello, L. Villani, and B. Siciliano, "A new laparoscopic tool with in-hand rolling capabilities for needle reorientation," *IEEE Robotics and Automation Letters*, vol. 3, no. 3, pp. 2354–2361, 2018.

[3] R. C. Jackson and M. C. Cavusoglu, "Needle path planning for autonomous robotic surgical suturing," *IEEE Int.Conference on Robotics and Automation*, pp. 1669–1675, 2013.

[4] R. C. Jackson, V. Desai, J. P. Castillo, and M. C. Çavuşoğlu, "Needle-tissue interaction force state estimation for robotic surgical suturing," *2016 IEEE/RSJ International Conference on Intelligent Robots and Systems (IROS)*, pp. 3659–3664, 2016.

[5] G. A. Fontanelli, L. Buonocore, F. Ficuciello, L. Villani, and B. Siciliano, "A novel force sensing integrated into the trocar for minimally invasive robotic surgery," *IEEE/RSJ Int. Conf. on Intelligent Robots and Systems*, pp. 131–136, 2017.

[6] S. Sen, A. Garg, D. V. Gealy, S. McKinley, Y. Jen, and K. Goldberg, "Automating multi-throw multilateral surgical suturing with a mechanical needle guide and sequential convex optimization," *IEEE Int. Conf. on Robotics and Automation*, pp. 4178–4185, 2016.

[7] A. Shademan, R. S. Decker, J. D. Opfermann, S. Leonard, A. Krieger, and P. C. W. Kim, "Supervised autonomous robotic soft tissue surgery," *Science Translational Medicine*, vol. 8, no. 337, 2016.

[8] J. Schulman, A. Gupta, S. Venkatesan, M. Tayson-Frederick, and P. Abbeel, "A case study of trajectory transfer through non-rigid registration for a simplified suturing scenario," *IEEE Int. Conf. on Intelligent Robots and Systems*, pp. 4111–4117, 2013.

[9] Z. Chen, A. Malpani, P. Chalasani, A. Deguet, S. S. V. Vedula, R. H. Taylor, and P. Kazanzides, "Virtual Fixture Assistance for Needle Passing and Knot Tying," *IEEE/RSJ Int. Conf. on Intelligent Robots and Systems*, pp. 2343–2350, 2016.

[10] B. Siciliano, L. Sciavicco, L. Villani, and G. Oriolo, *Robotics: Modelling, Planning and Control*. Springer, 2010.

[11] G. A. Fontanelli, F. Ficuciello, L. Villani, and B. Siciliano, "Modelling and identification of the da Vinci research kit robotic arms," *IEEE/RSJ Int. Conf. on Intelligent Robots and Systems*, pp. 1464–1469, 2017.

[12] M. Selvaggio, G. A. Fontanelli, F. Ficuciello, L. Villani, and B. Siciliano, "Passive virtual fixtures adaptation in minimally invasive robotic surgery," *IEEE Robotics and Automation Letters*, vol. 3, no. 4, pp. 3129–3136, 2018.

[13] A. De Luca and R. Mattone, "Sensorless robot collision detection and hybrid force/motion control," *Proceedings - IEEE Int. Conf. on Robotics and Automation*, vol. 2005, no. April, pp. 999–1004, 2005.

[14] Z. Zhang, L. Zhang, and G. Z. Yang, "A computationally efficient method for handeye calibration," *International Journal of Computer Assisted Radiology and Surgery*, vol. 12, no. 10, pp. 1775–1787, 2017.

[15] S. A. Bowyer, B. L. Davies, and F. Rodriguez Y Baena, "Active constraints/virtual fixtures: A survey," *IEEE Transactions on Robotics*, vol. 30, no. 1, pp. 138–157, 2014.

[16] P. Kazanzides, Z. Chen, A. Deguet, G. S. Fischer, R. H. Taylor, and S. P. DiMaio, "An open-source research kit for the da Vinci surgical system," *IEEE Int. Conference on Robotics and Automation*, pp. 6434–6439, May 2014.

[17] K. Kronander and A. Billard, "Stability considerations for variable impedance control," *IEEE Transactions on Robotics*, vol. 32, no. 5, pp. 1298–1305, Oct 2016.

[18] S. G. Hart, "Nasa-task load index (nasa-tlx); 20 years later," *The Human Factors and Ergonomics Society Annual Meeting*, vol. 50, no. 9, pp. 904–908, 2006.